Immunodeficiency, auto-inflammation and amylopectinosis in humans with inherited HOIL-1 and LUBAC deficiency

Citation	Boisson, B., E. Laplantine, C. Prando, S. Giliani, E. Israelsson, Z. Xu, A. Abhyankar, et al. 2012. "Immunodeficiency, auto-inflammation and amylopectinosis in humans with inherited HOIL-1 and LUBAC deficiency." Nature immunology 13 (12): 1178-1186. doi:10.1038/ni.2457. http://dx.doi.org/10.1038/ni.2457.
Published Version	doi:10.1038/ni.2457
Accessed	April 17, 2018 4:26:33 PM EDT
Citable Link	http://nrs.harvard.edu/urn-3:HUL.InstRepos:11708667
Terms of Use	This article was downloaded from Harvard University's DASH repository, and is made available under the terms and conditions applicable to Other Posted Material, as set forth at http://nrs.harvard.edu/urn-3:HUL.InstRepos:dash.current.terms-of-use#LAA

(Article begins on next page)

Immunodeficiency, auto-inflammation and amylopectinosis in humans with inherited HOIL-1 and LUBAC deficiency

Bertrand Boisson[1,*], **Emmanuel Laplantine**[2,*], **Carolina Prando**[1,*], **Silvia Giliani**[3,#], **Elisabeth Israelsson**[4,#], **Zhaohui Xu**[5,#], **Avinash Abhyankar**[1,#], **Laura Israël**[6,7], **Giraldina Trevejo-Nunez**[1], **Dusan Bogunovic**[1], **Alma-Martina Cepika**[5], **Donna MacDuff**[8], **Maya Chrabieh**[6,7], **Marjorie Hubeau**[6,7], **Fanny Bajolle**[9], **Marianne Debré**[10], **Evelina Mazzolari**[3], **Donatella Vairo**[3], **Fabrice Agou**[11], **Herbert W. Virgin**[8], **Xavier Bossuyt**[12], **Caroline Rambaud**[13], **Fabio Facchetti**[14], **Damien Bonnet**[7,9], **Pierre Quartier**[7,10], **Jean-Christophe Fournet**[7,15], **Virginia Pascual**[5,**], **Damien Chaussabel**[4,5,**], **Luigi D. Notarangelo**[16,**], **Anne Puel**[6,7,**], **Alain Israël**[2,##], **Jean-Laurent Casanova**[1,6,7,10,##], and **Capucine Picard**[6,7,10,17,##]

[1]St Giles Laboratory of Human Genetics of Infectious Diseases, Rockefeller Branch, Rockefeller University, NY, USA

[2]Laboratory of Molecular Signaling and Cell Activation, CNRS, URA 2582, Institut Pasteur, Paris, France, EU

[3]Laboratory of Genetic Disorders of Childhood and Pediatric Clinic, A. Nocivelli Institute for Molecular Medicine, Dept of Pathology, Spedali Civili and Pediatric Clinic, University of Brescia, Brescia, Italy, EU

[4]Benaroya Research Institute at Virginia Mason, Seattle, WA, USA

[5]Baylor Institute for Immunology Research and Baylor Research Institute, Dallas, Texas, USA

[6]Laboratory of Human Genetics of Infectious Diseases, Necker Branch, INSERM U980, Necker Medical School, Paris, France, EU

[7]Paris Descartes University, Sorbonne Paris Cité, France, EU

[8]Washington University School of Medicine and Midwest Regional Center of Excellence for Biodefense and Emerging Infectious Disease Research, Saint Louis, Missouri, USA

[9]Reference Center for Complex Congenital Heart Defects, Assistance Publique Hôpitaux de Paris (AP-HP), Necker Enfants Malades Hospital, Paris, France, EU

[10]Pediatric Hematology-Immunology-Rheumatology Unit, AP-HP, Necker Enfants Malades Hospital, Paris, France, EU

[11]Institut Pasteur, Structural and Cellular Biochemistry Unit, CNRS, URA 2185, France, EU

[12]Experimental Laboratory Immunology, Department of Microbiology and Immunology, Biomedical Science Group, Catholic University of Leuven, Leuven, Belgium, EU

[13]Pathology Laboratory, AP-HP, Raymond Poincarré, Garches, France, EU

[14]Department of Pathology, Spedali Civili and University of Brescia, Brescia, Italy, EU

[15]Pathology Laboratory, AP-HP, Necker Enfants Malades Hospital, Paris, France, EU

[16]Division of Immunology and The Manton Center for Orphan Disease Research, Children's Hospital, Harvard Medical School, Boston, MA, USA

[17]Study Center for Primary Immunodeficiencies, AP-HP, Necker Enfants Malades Hospital, Paris, France, EU

Abstract

We report the clinical description and molecular dissection of a new fatal human inherited disorder characterized by chronic auto-inflammation, invasive bacterial infections and muscular amylopectinosis. Patients from two kindreds carried biallelic loss-of-expression and loss-of-function mutations in *HOIL1*, a component the linear ubiquitination chain assembly complex (LUBAC). These mutations resulted in impairment of LUBAC stability. NF-κB activation in response to interleukin-1β (IL-1β) was compromised in the patients' fibroblasts. By contrast, the patients' mononuclear leukocytes, particularly monocytes, were hyperresponsive to IL-1β. The consequences of human HOIL-1 and LUBAC deficiencies for IL-1β responses thus differed between cell types, consistent with the unique association of auto-inflammation and immunodeficiency in these patients. These data suggest that LUBAC regulates NF-κB-dependent IL-1β responses differently in different cell types.

Auto-inflammatory disorders are characterized by immune system hyperactivation in the absence of autoantibodies, and self-reactive T cells [1]. The genetic dissection of several auto-inflammatory disorders has implicated two pro-inflammatory cytokines in these conditions: interleukin (IL)-1β and tumor necrosis factor (TNF) [2,3]. Autosomal dominant TNF receptor-associated periodic fever (TRAPS) was the first genetic etiology of auto-inflammatory disorders to be identified. It is caused by mutations in *TNFRSF1A*, resulting in the enhanced activation of mitogen-activated protein kinases (MAPKs) and the secretion of pro-inflammatory cytokines in response to lipopolysaccharide (LPS) [3]. Inflammasomopathies include autosomal dominant cryopyrin-associated periodic fever (CAPS, also known as chronic infantile neurological cutaneous and articular syndrome (CINCA)/neonatal-onset multisystem inflammatory disease (NOMID), Muckle Wells syndrome (MWS), familial cold autoinflammatory syndrome (FCAS)), caused by mutation of *NLRP3* (also known as *CIAS1*), autosomal recessive familial Mediterranean fever (FMF), caused by mutation of *MEFV*, autosomal recessive mevalonate kinase (MVK) deficiency, caused by mutation of *MVK*, autosomal recessive deficiency of the IL-1 receptor antagonist (DIRA), caused by mutation of *IL1RN,* and autosomal dominant pyogenic arthritis pyoderma gangrenosum and acne (PAPA) syndrome, caused by mutation of *CD2BP1*. The clinical phenotypes of these diseases result largely from enhanced IL-1β activity [2]. All these auto-inflammatory disorders are associated with recurrent episodes of fever, skin rash and aseptic organ inflammation and may be complicated by metabolic abnormalities (e.g. 30% of TRAPS patients develop amyloidosis) [1,3]. Patients with these diseases are not generally prone to unusual infectious diseases.

In sharp contrast, inborn errors decreasing TNF- and IL-1β-mediated immunity are associated with severe infectious diseases in the context of impaired inflammation. Inborn errors of NF-κB-mediated immunity are associated with impaired cellular responses to

various stimuli, including TNF and IL-1β; these diseases include X-linked recessive and autosomal dominant anhidrotic ectodermal dysplasia with immunodeficiency (EDA-ID), due to hypomorphic mutations of the NF-κB essential modulator (*NEMO*) gene and hypermorphic mutations of the *IKBA* gene, respectively [4–7]. Defects restricted to the Toll-like receptor and IL-1R (TIRs) pathway, affecting the NF-κB, IRF3 and MAPK signaling molecules, include autosomal recessive IRAK-4 and autosomal recessive MyD88 deficiencies [7–12]. Patients with these two deficiencies are prone to the development of life-threatening pyogenic bacterial diseases [10]. The range of infections is much broader in patients with NEMO and IκBα deficiencies [13]. A characteristic of these four inborn errors of immunity is that clinical and biological signs of inflammation are absent or delayed during infectious episodes, although they may reach normal levels during prolonged infection [13]. For example, the induction of IL-6-dependent C-reactive protein (CRP) is impaired in these patients [10,14]. We report here the description and investigation of three patients from two unrelated families displaying a paradoxical clinical phenotype combining auto-inflammatory syndrome and pyogenic bacterial diseases [15]. These patients also developed muscular amylopectinosis, consisting of intracellular glycogen inclusions, complicated by myopathy and cardiomyopathy, which have never previously been associated with any inborn error of immunity. These patients carry loss-of-function mutations in *HOIL1* (*RBCK1*), a component of the linear ubiquitination chain assembly complex (LUBAC). This E3 ligase complex, which adds head-to-tail linear polyubiquitin chains to substrate proteins, has been implicated in NF-κB signaling [16,17].

Results

HOIL1 germline mutations in patients from two kindreds

The first kindred investigated (kindred A, French) was not consanguineous, but we nonetheless hypothesized that the two sisters (P1 and P2) suffered from an autosomal recessive disorder (Fig. 1a, case reports in supplementary note and Supplementary Fig. 1). We set out to decipher the underlying genetic defect by two genome-wide (GW) approaches: use of a GW human high-density SNP array (genome-wide investigations; GWI) to search for large genetic lesions, including, copy number variations (CNV) in particular; and a whole-exome sequencing (WES) approach to search for small genetic lesions, including coding gene variations in particular [18–20]. No homozygous candidate lesion was identified by either approach, suggesting that the two patients might be compound heterozygous. We therefore searched for heterozygous lesions in the same gene by GWI and WES. In both patients, we found a single-copy loss of 31.799 kb on chromosome 20p.13, encompassing the three last exons of *TRIB3* and the first four exons of *HOIL1* (also known as *RBCK1*) (Fig. 1b). This deletion resulted from a genomic rearrangement due to non allelic homologous recombination between intron 1 of *TRIB3* and intron 4 of *HOIL1* (named *TRIB3*:g.-1272_*HOIL1*:g.9780del) (Supplementary Fig. 2a,b). The lesion was inherited from the mother and was not transmitted to the healthy siblings. No other mutation in *TRIB3* was identified by WES or Sanger sequencing. By contrast, WES and Sanger sequencing both showed that the two patients were heterozygous for the paternally derived nonsense p.Q185X (c.553C>T) mutation in exon 5 of *HOIL1* (Fig. 1c).

The second kindred investigated (kindred B, Italian) is consanguineous. The search for large genetic lesions by GWI was not informative (Fig. 1a, case report in supplementary note). By contrast, a homozygous deletion of CT at positions 121 and 122 (c.121_122delCT) in exon 2 of *HOIL1* was identified in P3 by WES and confirmed by Sanger sequencing. This deletion resulted in a frameshift (fs) and a premature stop codon (p.L41fsX7) (Fig. 1d). GW linkage (GWL) and homozygosity mapping showed that the *HOIL1* gene was located in a chromosomal region linked to the disease (data not shown). Both parents and one healthy sibling were heterozygous for the mutation. The three *HOIL1* variants found in the two

kindreds were not found in public databases (NCBI, UCSC, 1000 genomes) or in our own GWI and WES databases of 124 and 621 individuals, respectively. They were also absent from the 392 individuals of the CEPH-HGD panel tested, suggesting that they are not irrelevant polymorphisms. *HOIL1* encodes hemoxidized iron-regulatory protein 2 ubiquitin ligase-1 (HOIL-1). HOIL-1 is one of the components of the linear ubiquitin chain assembly complex (LUBAC), an E3 ligase complex that adds head-to-tail linear polyubiquitin chains to substrate proteins [16,17]. The large deletion in HOIL-1 in P1 and P2 was predicted, at the very least, to result in the deletion of the ubiquitin-like (Ubl) domain (assuming that translation is reinitiated; Fig. 1e). The small nucleotide deletion in the gene in P3 was predicted to result in the deletion of all functional domains of HOIL-1. The nonsense mutation in P1 and P2 was predicted to result in premature truncation within the novel zinc finger (NZF) domain of HOIL-1. The Ubl domain is required for LUBAC formation and linear ubiquitination [16]. Collectively, these genetic data suggest that P1 and P2 from kindred A are compound heterozygous, and P3 from kindred B is homozygous, for rare deleterious alleles of *HOIL1*.

Impaired HOIL-1 expression in the patients' cells

We assayed *TRIB3* and *HOIL1* mRNA by reverse transcription-quantitative PCR (RT-qPCR) in SV40-transformed fibroblasts from patients and controls. The amounts of *TRIB3* mRNA were normal in the patients' cells (data not shown), whereas the amounts of *HOIL1* mRNA were one third to a quarter those in the controls (Fig. 2a). Similarly, TRIB3 protein was present in the patients' cells (Fig. 2b), whereas HOIL-1 was undetectable by immunoblotting with antibodies directed against the N-terminal (Fig. 2b) or C-terminal part of the protein (data not shown). HOIL-1 was also not detectable in EBV-transformed B cell lines (EBV-B cells) derived from P2 (data not shown). LUBAC is thought to consist of three protein subunits: HOIL-1, SHANK-associated RH domain-interacting protein (SHARPIN,), and HOIL-1 interaction protein (HOIP, also known as RNF31) [17,21–24]. We thus assessed the abundance of these three components of LUBAC in fibroblasts. In cells from the three patients, SHARPIN protein levels were about 50 % lower than those in control cells (Fig. 2c) and HOIP was almost undetectable (Fig. 2c). It was therefore not possible to co-immunoprecipitate SHARPIN with HOIP in cells from P1 (Fig. 2d). No lesion in *HOIP* or *SHARPIN* was detected by GWI and WES in the three patients. We then used the patients' fibroblasts (P1, P2) to investigate whether the expression of a wild-type (wt) *HOIL1* allele rescued LUBAC expression: HOIL-1 production was restored in the patients' cells by stable transfection with wt *HOIL1* (Fig. 2e). This re-expression of HOIL-1 also restored expression of the other two LUBAC components, HOIP and SHARPIN, to control levels (Fig. 2e). These findings formally demonstrate that HOIL-1 is required for the overall stability of LUBAC. Cells from the two compound heterozygous patients (P1 and P2) and from the patient homozygous (P3) for *HOIL1* mutations therefore displayed HOIL-1 deficiency, resulting in a large decrease in the levels of the other two molecules normally present in LUBAC.

Impaired NF-κB activation in the patients' fibroblasts and B cells

It has been suggested that, at least on some cell types, LUBAC regulates activation of the canonical NF-κB pathway, which plays a key role in inflammatory and immune responses. We therefore assessed the functionality of the canonical NF-κB pathway in SV40-transformed fibroblasts from the patients. The lack of HOIL-1 in the patients' cells led to lower levels of IKK kinase phosphorylation, slower IκBα degradation and a decrease in NEMO ubiquitination in response to stimulation with either TNF or IL-1β (Fig. 3a,b). By contrast, JNK phosphorylation in response to both stimuli was normal in the patients' fibroblasts (Fig. 3a,b). The lower levels of NF-κB activation in the patients' cells were associated with lower NF-κB transcriptional activity, as assessed by NF-κB-reporter assays

(Supplementary Fig. 3a). This impairment of the canonical NF-κB pathway led to weak induction of the NF-κB target genes *IL6* and *A20*, which are normally induced by TNF or IL-1β (Supplementary Fig. 3b). Consistent with these RT-qPCR data, IL-6 production, as assessed by ELISA, in response to TNF or IL-1β treatment was weak in cells from the patients (Fig. 3c and Supplementary Fig. 4a,b), and the response to IL-1β was more severely impaired than that to TNF. The induction of the NF-κB target gene products cIAPs (cellular inhibitors of apoptosis) was weaker in cells from P2 than controls, and higher levels of caspase-3 cleavage were observed in response to stimulation with TNF (Supplementary Fig. 4c). These observations indicated that *HOIL1*-deficient cells were more susceptible than controls to TNF-induced apoptosis. The re-introduction of wt HOIL-1 into P1 fibroblasts restored IKK kinase phosphorylation, IκBα degradation and IL-6 secretion in response to both TNF and IL-1β (Fig. 3d-f). This confirmed that the *HOIL1* mutant alleles in the patients' fibroblasts were responsible for the impairment of the NF-κB response to both TNF and IL-1β. Analysis of IL-6 production by the patients' fibroblasts following stimulation with TLR2, TLR6 or TLR4 agonists indicated that these TLR pathways were also partially affected (Supplementary Fig. 4d). IFN-β production following stimulation with the TLR3 agonist poly(I:C) was abolished in fibroblasts from the patients, whereas stimulation of the RNA helicase RIG-I with 7SK-AS or poly(I:C) plus Lipofectamine was normal (Supplementary Fig. 4e). Likewise, stimulation with R-848 (a TLR7 and a TLR8 agonist) completely failed to induce TNF production by the patients' EBV-B cells (Supplementary Fig. 5a). Finally, IKK phosphorylation and IκBα degradation in response to both IL-1β and CD40L were abolished in EBV-B cell lines from P2 (Supplementary Fig. 5b,c). Overall, NF-κB responses to all tested agonists of tumor necrosis factor receptor (TNFR), IL-1R and TLR family members were impaired in fibroblasts and EBV-B cells from patients with HOIL-1 deficiency.

Impaired NEMO recruitment to cytokine receptors

We investigated the molecular mechanisms underlying the defects in NF-κB activation in HOIL-1-deficient fibroblasts. It has been suggested that LUBAC regulates NF-κB activation by stabilizing the recruitment of the NEMO-IKK complex to the cytokine-activated receptor [16,21,23,25–27]. We therefore investigated the consequences of HOIL-1 deficiency for NEMO recruitment to the TNF- and IL-1-R signaling complexes (RSCs). In control cells, NEMO was rapidly and transiently recruited to the RSCs, and a clear enrichment in ubiquitinated NEMO species was observed (Fig. 4a,b). However, in cells from the HOIL-1-deficient patients, less NEMO was recruited to the TNF-RSC (particularly for the ubiquitinated NEMO species) (Fig. 4a) and NEMO recruitment to the IL-1-RSC was almost entirely abolished (Fig. 4b). SHARPIN recruitment to the RSCs was also reduced, especially in response to IL-1β (data not shown). We then investigated the association between NEMO and the polyubiquitinated adapter RIP1 in response to TNF and between NEMO and the polyubiquitinated adapter IRAK-1 in response to IL-1β. Less NEMO was associated with ubiquitinated forms of RIP1 in patient-derived than control fibroblasts, whereas the amount of polyubiquitinated RIP1 present in the TNF-RSC was normal (Fig. 4c). Similarly, the interaction between NEMO and ubiquitinated IRAK-1 in response to IL-1β was strongly impaired in the patients' cells, although the ubiquitination of IRAK-1 was unaffected (Fig. 4d). Thus, the absence of HOIL-1 affects the recruitment or stability of NEMO-IKK complexes in response to both TNF and IL-1β, with the most severe defect being observed for the IL-1-RSC.

Genome-wide impact of HOIL-1 deficiency in fibroblasts

These findings are generally consistent with the high incidence of opportunistic infections in the *HOIL1*-deficient patients, which was similar to that of patients with impaired IL-1R- and/or TNFR-dependent NF-κB immunity [5–7,13]. However, unlike patients with these other

immunodeficiencies, HOIL-1-deficient patients also presented with auto-inflammation and amylopectinosis. We therefore investigated the effects of HOIL-1-deficiency on TNF and IL-1β responses, by analyzing the GW transcriptional profiles (47,231 probes) of primary fibroblasts from four healthy controls, three HOIL-1-deficient patients (P1, P2 and P3), one *MyD88*-deficient patient and one *NEMO*-deficient fetus. In control fibroblasts, 544 and 2,208 transcripts were regulated by IL-1β after 2 hours and 6 hours of stimulation, respectively, and 456 and 1,614 transcripts were regulated by TNF at the same time points (Fig. 5). NEMO-deficient cells did not respond to either stimulus, whereas, as expected, MyD88-deficient cells responded to TNF but not to IL-1β. By contrast, HOIL-1-deficient cells were poorly responsive to IL-1β, as assessed after 2 h and 6 h; the response to TNF was almost identical to that of control cells after 2 h, but was weaker than that of control cells after 6 h. A more detailed analysis showed that control fibroblasts responded to IL-1β and TNF by the rapid induction of inflammatory cytokines, chemokines and cell surface receptors (e.g. the *CCL5, CCL8, CXCL1, CXCL2, CXCL10, CXCR7, IL1β,* and *TNFAIP3* (also known as *A20*) genes). The upregulation of these transcripts after 6 h of IL-1β stimulation was generally blunted in patients with HOIL-1 deficiency, although there were a few notable exceptions (e.g. *CCL2*, *CXCL1*, *IL8* and *IL32*). Thus, HOIL-1 deficiency in human fibroblast cells results in the impaired expression of NF-κB-target genes in response to IL-1β and, to a lesser extent, TNF. The GW transcriptome analysis data for fibroblasts were therefore consistent with the *in vitro* investigations described above and, in particular, with the receptor recruitment data (Fig. 4a,b): HOIL-1 deficiency and NEMO deficiency shared many similarities, with only a few differences in terms of the fibroblast response to IL-1β, whereas the responses to TNF were more discordant.

Genome-wide impact of HOIL-1 deficiency in leukocytes

We studied the basis of auto-inflammation in the patients further, by investigating their leukocytes *ex vivo*. We first investigated the consequences of HOIL-1-deficiency, by analyzing the GW transcriptional profiles of whole blood cells from P1 (without acute phase and free of infection) in the absence of stimulation. We compared the transcriptional profile of P1 with those of 41 healthy age-matched children and other patients with various genetically determined auto-inflammatory disorders, including CAPS disorders (CINCA (2 patients) and Muckle-Wells syndrome (MWS, 5 patients)) and MVK deficiency (2 patients). Blood cells from P1 had a unique gene expression profile (Fig. 6a and Supplementary Fig. 6a,b), with 2,900 transcripts up- or downregulated by a factor of at least two with respect to healthy controls. Transcripts encoding HOIL-1, IFN-γ and several members of the TNF family including CD30L (also known as TNFSF8) and APRIL (also known as TNFSF13) were downregulated by a factor of at least two. Transcripts encoding the pro-inflammatory cytokines IL-6, IL-6R and IL-6ST were upregulated in the patient's blood *ex vivo* (Supplementary Fig. 6b). Genes belonging to networks involved in cell death, the cell cycle and cell signaling, the inflammatory response, immune cell trafficking and carbohydrate metabolism were identified as being dysregulated in the patient. Using a pre-established framework of transcriptionally coregulated transcripts, we demonstrated a distinct upregulation of erythroid lineage- and ubiquitination-related transcripts that differentiated the pattern of gene expression in the blood cells from this patient from those of patients with *NLRP3* and *MVK* mutations (Supplementary Fig. 6a). We also retrospectively studied the concentrations of inflammatory markers and cytokines in plasma samples collected from P1 and P2 at various ages. Consistent with the clinical phenotype, background concentrations of C-reactive protein (CRP) and IL-6 were high, increasing further during each inflammatory episode (Fig. 6b). The concentrations of other pro-inflammatory cytokines, including IL-8, TNF and IL-1β, and of some anti-inflammatory cytokines, notably the IL-1R antagonist, were also high (Fig. 6b and data not shown). We then used ELISA to study the production of cytokines by whole blood cells from P1 and P2 in response to stimulation (IL-1β, TLR

agonists, two heat-killed pneumococcus strains and TNF). IL-1β and agonists of TLR1 and TLR2 induced IL-6 production in both patients more strongly than in healthy controls, whereas IL-10 production in response to treatment with TNF was abolished (Fig. 6c,d and Supplementary Fig. 6c). Therefore, by contrast to the phenotype seen with fibroblasts, leukocytes from these two HOIL-1-deficient patients appeared to be both constitutively hyperinflammatory and hyperresponsive to IL-1β (but probably not TNF) *ex vivo*; this may explain, in part, the patients' auto-inflammatory syndrome *in vivo*.

Hyperactivation of HOIL-1-deficient mononuclear leukocytes

We further investigated the inflammatory phenotype observed in whole blood cells from HOIL-1-deficient patients. We analyzed the GW transcriptional profiles of peripheral blood mononuclear cells (PBMCs) from the three patients (P1, P2, P3), three healthy controls (including two age-matched controls (C2 and C3)) and two MyD88-deficient patients stimulated with TNF or IL-1β. The transcriptional profiles of PBMCs from HOIL-1-deficient patients, healthy controls and MyD88-deficient patients were similar following TNF stimulation (Fig. 7a-left panel). However, in response to IL-1β, *HOIL1*-deficient PBMCs displayed an overinduction, with respect to healthy controls, of the transcription of 19 and 12 genes at 2 h and 6 h, respectively (Fig. 7a-right panel). As expected, leukocytes from *MyD88*-deficient patients were unresponsive to IL-1β. The genes hyperinduced by IL-1β in *HOIL1*-deficient cells included genes encoding pro-inflammatory cytokines: *IL6*, *MIP1A*, *MIP1B*, *IL8* and *IL1B* (Fig. 7b). We then investigated which PBMC subsets were responsible for this hyperresponse to IL-1β in HOIL-1-deficient patients. PBMCs from P2, seven healthy controls and one IRAK-4-deficient patient were stimulated with TNF, IL-1β, LPS or PMA+ionomycin+CpG-B. The various PBMC subsets were identified according to the cell surface expression of the following markers: CD3 (T cells), CD19 (B cells), CD56 (NK cells) and CD14 (monocytes). The production of IL-6, IL-8, MIP-1α, MIP-1β, IL-1β and IFN-γ was assessed by intracellular staining and flow cytometry. In the CD3^{+}, CD19^{+} and CD56^{+} cells from the controls, HOIL-1- and IRAK-4-deficient patients, no response to TNF or IL-1β stimulation was observed (Supplementary Fig. 7a and data not shown). Upon stimulation with PMA+ionomycin+CpG-B, CD3^{+} cells from P2 produced large amounts of IL-8 (11% CD3^{+}IL-8^{+} vs. 4% ± 3.8% in controls) whereas IFN-γ was produced in smaller amounts (1% CD3^{+}IFN-γ^{+} vs. 15%±7.3, Supplementary Fig. 7a). Monocytes from P2 produced four times more IL-6 than those from healthy controls upon IL-1β stimulation, whereas IRAK-4-deficient monocytes were unresponsive (Fig. 7c, upper panels and Supplementary Fig. 7b). Monocytes from P2 also produced large amounts of MIP-1α (Fig. 7c, middle panels), but the levels of IL-8, IL-1β and MIP-1β production were similar to control values (Fig. 7c, lower panel and Supplementary Fig. 7a,b). Finally, healthy controls and P2 monocytes responded similarly to LPS in terms of IL-6, IL-1β, and MIP-1α production (Fig. 7c, upper panel and Supplementary Fig. 7a). In conclusion, the hyperresponse of whole blood and PBMCs from HOIL-1-deficient patients to IL-1β appears to be a consequence of the hyperresponsiveness of monocytes, probably accounting for the clinical auto-inflammation in these patients.

Discussion

We have identified autosomal recessive HOIL-1 deficiency as the cause of a new clinical entity combining invasive pyogenic bacterial infections, systemic auto-inflammation and amylopectin-like deposits in muscle. HOIL-1, SHARPIN and HOIP are the three components of LUBAC [17,22–24]. SHARPIN and HOIP protein levels are low in the absence of HOIL-1 and their restoration following HOIL-1 re-expression suggests that LUBAC is a ternary complex. HOIP, the catalytic center of LUBAC [16,17], was almost undetectable in fibroblasts and B cells from HOIL-1-deficient patients, suggesting that these patients are

LUBAC-deficient. LUBAC is involved in the NF-κB pathway and conjugates linear polyubiquitin chains onto specific Lys residues of NEMO [16]. HOIL-1-deficient human fibroblasts displayed impaired NF-κB activation, resulting in impaired NF-κB-driven gene transcription and cytokine production in response to TNF and IL-1β, consistent with data in mouse *Hoil1* knockdown or knockout cells [16,27]. However, TNF- and IL-1β-induced JNK activity was normal in *HOIL1*-deficient human fibroblasts, whereas TNF-induced JNK activity was enhanced in *Hoil1*^{−/−} mouse embryonic fibroblasts (MEFs) [16,26]. Overall, our results demonstrate that human HOIL-1 and LUBAC are required for TNF- and IL-1β-induced NF-κB responses, at least in fibroblasts.

LUBAC facilitates the recruitment of the NEMO-IKK complex to cytokine receptors, in at least some cell types [27,29]. We showed that the recruitment of human NEMO to TNF- and IL-1-RSCs was compromised in HOIL-1-deficient fibroblasts. LUBAC-mediated linear ubiquitination may facilitate the activation of IKK kinases; presumably, the attachment of linear ubiquitin chains to NEMO [16] and, possibly, other components of the RSC [23] favors or stabilizes the incorporation of NEMO into the RSCs. The recognition of these linear ubiquitin chains by NEMO itself and, probably, by other components of the NF-κB cascade may then lead to a local accumulation of IKK kinases, favoring their trans-phosphorylation and activation. Alternatively, NEMO ubiquitination may induce a conformational change required for activation of the associated kinases. However, the levels of NEMO ubiquitination in response to TNF or IL-1β in the patients' cells were only slightly lower than those in control cells, whereas the amount of ubiquitinated NEMO recruited to the TNFR or IL-1R correlated strongly with the signaling defect, as demonstrated by transcriptome analysis. Our findings also suggest that human LUBAC is required for optimal responses to other members of the TIR family, such as TLR3, and of the TNFR family, such as CD40.

The susceptibility of these patients to invasive pyogenic bacterial disease is probably due to impaired NF-κB-dependent responses to at least some key members of the TIR and TNFR families in fibroblasts and, possibly, other cell types. Indeed, patients with inborn errors of NF-κB-mediated or TIR-mediated immunity, carrying IκBα, NEMO, IRAK-4 or MyD88 mutations, are also prone to pyogenic bacterial infections [5,6,8,9,13]. The infectious phenotype of MyD88- and IRAK4-deficient patients is narrower than that of most patients with NEMO or IκBα mutations [7,10,13]. It may not be coincidental that IRAK-4-, MyD88- and HOIL-1-deficient patients share a profound lack of response to TIRs and predisposition to pyogenic bacterial diseases. One of the HOIL-1-deficient patients (P3) had a persistent cytomegalovirus infection, but it is unclear whether this was a consequence of HOIL-1 deficiency. Unlike most IRAK-4- and MyD88-deficient patients, patients bearing mutations in *NEMO* and *HOIL1* are deficient in memory B cells and their antibody response to pneumococcal glycans is impaired . Two patients died before hematopoietic stem cell transplantation (HSCT) and the third died too soon after HSCT for any firm conclusions to be drawn about a possible hematopoietic origin of the predisposition to infection, as in patients with NEMO and IκBα deficiencies [13]. Similarly, *Hoil1*^{−/−} and *Sharpin*-deficient (Sharpin[cpdm]) mice are uninformative on this issue, as neither has been challenged with pathogens [16,22–24,30].

Bacterial infections in patients with mutations in IκBα, NEMO, IRAK-4 or MyD88 are associated with impaired inflammation [5–7,10,13,31], at odds with HOIL-1-deficient patients, who even displayed inflammation in the absence of overt infection. The auto-inflammatory phenotype of our patients is consistent with that of their mononuclear leukocytes, monocytes in particular, which display constitutive over-transcription of numerous inflammatory genes and are hyperresponsive to IL-1β[1–3]. The hematopoietic origin of the auto-inflammation in HOIL-1-deficient patients is further supported by the fact that inflammation was controlled

following HSCT in one HOIL-1-deficient patient. In the mouse, LUBAC seems to modulate inflammatory responses by regulating NF-κB activation directly [16,17,21,23,25–27] and *Hoil1-* deficient mice display no apparent excessive inflammation [24]. However, Sharpin*cpdm* mice [22- 24,30,33] display severe eosinophilic inflammation and defective lymphoid organogenesis [22–24,33–36]. Consistent with this, the inflammatory disease in Sharpin*cpdm* mice is partially rescued by inactivation of the *IL1RAP* gene[36], implicating IL-1β. The inflammatory phenotype of HOIL-1-deficient patients therefore resembles that of Sharpin*cpdm* mice. Furthermore, inactivation of the *TNF* gene improves skin lesions in Sharpin*cpdm* mice [23] and anti-TNF antibody treatment in one HOIL-1-deficient patient reduced the clinical inflammation. This improvement might have resulted from a decrease in TNF-mediated IL-1β activity. Our study reveals that human HOIL-1 is anti-inflammatory: patients lacking HOIL-1 display a strong auto-inflammatory phenotype.

Auto-inflammatory disorders may be complicated by metabolic disorders, with TRAPS patients often developing amyloidosis, for example [1,3]. The HOIL-1-deficient patients displayed no amyloidosis, but had amylopectinosis, in the form of intracellular glycogen inclusions in their muscles. Amylopectinosis has not been reported in *Sharpin*cpdm* and *Hoil1*^{−/−}mice [16,22–24,34]. Several genetic etiologies of human amylopectinosis have been reported [41–43]. HOIL-1 deficiency is a novel cause of amylopectinosis involving unknown mechanisms probably independent of IL-1, TNF and NF-κB, as amylopectinosis is not seen in other disorders associated with enhanced or impaired NF-κB immunity [5–7,13]. In conclusion, the patients described here display a unique combination of clinical phenotypes, highlighting the important and complex role of LUBAC in inflammation, immunity and metabolism in humans. The paradoxical association of auto-inflammation and immunodeficiency probably results from an imbalance between cellular responses, to NF-κB-dependent pro-inflammatory stimuli at least, mediated by TIRs and TNFRs in particular. The molecular basis of the immunodeficiency may be impaired responses to inflammatory stimuli in fibroblasts, and possibly other non-hematopoietic cell types, whereas the auto-inflammation may result from enhanced responses to IL-1β in leukocytes, including monocytes in particular.

Methods

Sample collection

This study was conducted in accordance with the Helsinki Declaration, with informed consent obtained from each patient or the patient's family. The study was approved by the local ethics committee of Necker-Enfants Malades Hospital, Paris, France, Spedali Civili and Pediatric Clinic, University of Brescia, Brescia, Italy, and the Rockefeller University Hospital, New York, USA.

Genetic analysis

Massively parallel sequencing—Genomic DNA extracted from the patient's peripheral blood cells was sheared with a Covaris S2 Ultrasonicator. An adapter-ligated library was prepared with the Paired-End Sample Prep kit V1 (Illumina). Exome capture was performed with the SureSelect Human All Exon kit (Agilent Technologies). Single-end sequencing was performed on an Illumina Genome Analyzer IIx, generating 72-base reads.

Sequence alignment, variant calling and annotation—Sequences were aligned with the human genome reference sequence (hg18 build), using BWA aligner [44]. Downstream processing was carried out with the Genome analysis toolkit (GATK) [45], SAMtools [46] and Picard Tools (http://picard.sourceforge.net). Substitution and indel calls were identified with a GATK UnifiedGenotyper and a GATK IndelGenotyperV2, respectively. All calls with a

read coverage 2× and a Phred-scaled SNP quality of 20 were filtered out. All the variants were annotated with the GATK Genomic Annotator.

Genome-wide human SNP array—Genomic DNA was isolated from the peripheral blood of two patients, a healthy sister and parents, by the phenol/chloroform method. The GeneChip Genome-Wide Human SNP Array 6.0 (Affymetrix) oligonucleotide-based array was used. Data were analyzed with Affymetrix Genotyping Console 4.0 software and the Affymetrix Genotyping Console Browser. The break points of the deletion on chromosome 20 were determined by PCR, with primers binding to intron 1 of *TRIB3* (aattgactggaagatcctgacg) and intron 5 of *HOIL1* (ggtacctccagcttccatctgg), flanking the deleted regions. PCR products were sequenced on an ABI 3130× sequencer.

Cell lines, immortalization and complementation

Control and patient-derived fibroblasts were immortalized by transfection with a plasmid expressing SV40 large-T antigen. Transformed cell lines were grown in DMEM (Gibco) supplemented with 10% fetal calf serum (Gibco). The *NEMO*$^{-/-}$ fibroblasts were kindly provided by Asma Smahi [47]. *HOIL1* mRNA was reverse-transcribed, amplified and inserted into the retroviral vector pMSCV (Clontech). Infectious viral particles were produced by cotransfecting GP2-293 packaging cells with pVSV-G and pMSCV-HOIL-1 or an empty vector (Clontech). Viral particles were collected 48–72 hours after transfection and used to infect SV40-transformed fibroblasts. Infected cells were selected with 0.4 μg/ml puromycin (Invitrogen).

Antibodies and reagents

The antibodies used for detection on immunoblots were anti-HOIL-1 N-ter (provided by Henning Walczak) [27], anti-HOIL-1 C-ter (provided by Kazuhiro Iwai) [21], anti-TRIB3 (2488-1, Epitomics), anti-HOIP (PAB6229, Abnova), anti-NEMO (sc-8330, Santa Cruz and #611306, BD), anti-SHARPIN (14626-1-AP, ProteinTech), anti-IκBα (#610690, BD), anti-phospho-IKKα-β (ser176/180) (16A6, Cell Signaling), anti-IKKβ (AM8109a, Abgent), anti-phospho-JNK (G-7, Santa Cruz), anti-JNK (sc-571, Santa Cruz), anti-IRAK1 (sc-7883 and sc-5288, Santa Cruz), anti-RIP1 (#610458, BD), anti-IL-1R1 (04-465, Millipore), anti-TNF-R1 (H-5, Santa Cruz), anti-cIAP (MAB3400, R&D Systems), anti-cleaved caspase-3 (Asp175) (9661, Cell Signaling), anti-β-tubulin (T4026, Sigma-Aldrich) and anti-GAPDH (sc-81545, Santa Cruz) antibodies. Species-specific secondary antibodies coupled to horseradish peroxidase were obtained from Vector Laboratories or Amersham-Pharmacia.

Cell lysis, immunoprecipitation and immunoblotting

Cells were lysed in a buffer containing 30 mM Tris-HCl pH 7.5, 120 mM NaCl, 2 mM KCl, 1% Triton X-100 and 2 mM EDTA supplemented with protease and phosphatase inhibitors (Complete and PhoStop, Roche). For immunoprecipitations, antibodies (5 μg) were added to 1 mg of total protein extract and incubated overnight at 4°C. Protein-A or protein G agarose beads (Sigma-Aldrich) were added to the samples, which were then incubated for 1 hour at 4°C. For experiments involving Flag-TNF and Flag-IL1-β treatments, cleared supernatants were incubated with anti-Flag M2 affinity gel (Sigma-Aldrich) for 2 hours at 4°C. For experiments involving biotinylated TNF treatments, cleared supernatants were incubated with streptavidin-agarose (Sigma-Aldrich) for 2 hours at 4°C. In all cases, beads were washed three times with lysis buffer and resuspended in Laemmli buffer. Proteins were separated by SDS–PAGE and transferred to PVDF membranes. Immunoreactive proteins were visualized by chemiluminescence. The relative amounts of HOIP and SHARPIN were determined with Quantity One software (Bio-Rad). For NF-κB-dependent reporter assays, SV40-transformed fibroblasts were transiently transfected with the NF-kB-dependent firefly

luciferase plasmid pGL4.32 (Promega) and the *Renilla* luciferase plasmid as an internal control, in the presence of Lipofectamine™ LTX reagent (Invitrogen). After 24 hours, cells were stimulated with TNF or IL-1β for four hours and luciferase activities were assessed with the dual luciferase assay kit (Promega).

Gene expression and microarray analysis

RNA was extracted from SV40-transformed fibroblasts with Trizol (Invitrogen) and reverse-transcribed (2 μg) with the SuperScript III first-strand synthesis kit (Invitrogen). *HOIL1*, *TRIB3*, *A20* and *IL6* mRNAs were quantified by RT-qPCR in a TaqMan Gene Expression Assay, with normalization against *GUS* probes.

Data acquisition—Whole blood cells from patients and healthy donors were collected and total RNA was extracted using the MagMAX-96 Blood RNA Isolation Kit (Applied Biosystems). Primary fibroblasts and PBMCs from patients and healthy donors were stimulated with IL-1β or TNF for 2 or 6 hours. Total RNA was isolated from fibroblasts and PBMCs with the RNeasy Mini Kit (Qiagen). RNA integrity was assessed on an Agilent 2100 Bioanalyzer. Biotinylated cDNA targets were prepared with the Illumina TotalPrep RNA Amplification Kit (Ambion) and hybridized to Illumina human HT-12 Expression Microarray Chips.

Data preprocessing—For the analysis, the background was subtracted and the raw signal values were extracted with Beadstudio v2 software (Illumina) and scaled by quantile normalization. The minimum intensity was set to 10, and all the intensity values were log2-transformed. Only the probes called as present in at least one sample ($p<0.01$) were retained for downstream analysis ($n=26,607$).

Data analysis—Raw data were first subjected to background subtraction and scaled to the average with Genome studio software (Illumina). They were then analyzed with Genespring software (Agilent). The minimum intensity was set to 10, and the intensity values were log2-transformed. For the analysis of *ex-vivo* whole blood samples, all samples were normalized with respect to the median intensity for control samples. After filtering out non-expressing probes, at least a two-fold difference in expression between patient 1 and 41 healthy controls was observed for 2,900 transcripts. A pre-established set of transcriptional modules was used as a framework for microarray data analysis. The approach used to construct this framework has been described elsewhere [48]. Genes with coordinated expression within or across nine human disease datasets were selected in multiple rounds of clique and paraclique clustering, to form a transcriptional module framework. The percentage of transcripts significantly up- or downregulated with respect to healthy controls ($p<0.05$, assuming equal variance) in each module was visualized on module maps. For the analysis of primary fibroblasts, transcripts without detectable expression changes (difference in normalized expression of less than 2-fold in either direction, in all samples) or absent from the dataset (as defined by an Illumina detection *p*-value greater than 0.01 in all samples) were filtered out, leaving 13,693 transcripts for downstream analysis. Stimulated samples from each donor were normalized with respect to their non stimulated reference sample. We identified the genes differentially regulated upon IL-1β or TNF stimulation in healthy donors on the basis of transcripts displaying a change in signal intensity of at least two-fold (up- or downregulation) with respect to the non stimulated control. We then investigated the expression of these genes in samples from the patients.

Cell stimulation, ELISA and FACS analysis

Cells were stimulated with the following cytokines and agonists: TNF, biotinylated-TNF and IL-1β (R&D Systems), Flag-TNF and Flag-IL1β (Alexis Biochemicals), Mega-CD40L

(Enzo), LPS (Sigma-Aldrich), phorbol-12-myristate-acetate (Sigma-Aldrich), ionomycin (Sigma-Aldrich) and CpG-B (Invivogen). For cytokine production by whole blood cells, blood was first mixed with an equal volume of RPMI, left untreated for 48 hours and then treated with cytokines or agonists for the indicated time. IL-6 and IL-10 secretion levels were determined with ELISA kits (M9316 and M1910, Sanquin).

Frozen PBMCs were washed twice with FCS-containing medium and used to seed 48-well plates (10^6 cells/well). They were cultured for 4–6 hours and then stimulated with TNF (20 ng/ml), IL-1β (10 ng/ml), LPS (10 ng/ml) or PMA+ionomycin+CpGB (10^{-9} M/10^{-7} M/100 μg/ml). Concomitantly to stimulation, protein transport was blocked with GolgiStop and GolgiPLug (BD). Cells were stained with anti-CD3 (BD, #560366), anti-CD19 (BD, #340951), anti-CD14 (BD, #557742), anti-CD56 (Biolegends, #318331) antibodies for cellular phenotyping and with Aqua Live/Dead (Invitrogen) to exclude dead cells. After fixation and permeabilization (BD, #554722), the cells were stained with antibodies against IL6 (BD, #561441), MIP-1α (BD, #554730), MIP-1β (BD, #560565), IL-1β (BD, #340515), IL-8 (BD, #511410) and IFN-γ (BD, #559326). Stained PBMCs were captured by flow cytometry with a BD LSRII flow cytometer and FACS Diva software. The data were analyzed with FlowJo (© Tree Star).

Histology and immunohistochemistry

Samples from the gut, heart and skeletal muscles of patients and healthy controls were studied. All cases were reviewed by two expert pathologists to confirm diagnosis. Formalin-fixed paraffin-embedded tissue blocks were cut into 4-μm sections that were stained with hematein-eosin (HE) and periodic acid-Schiff (PAS) reagent before and after diastase digestion. Images were acquired with a Leica DM LB2 microscope at a magnification of ×400 and a Leica DFC 280 camera. Slides were digitized with a Hamamatsu Nanozoomer.

Statistics

GraphPad Prism software was used to conduct unpaired, two-tailed Student's *t* tests for sample analysis or one-way ANOVA followed by Tukey's multiple comparison test. Values of $p < 0.05$ were considered significant.

Supplementary Material

Refer to Web version on PubMed Central for supplementary material.

Acknowledgments

References

1. Masters SL, Simon A, Aksentijevich I, Kastner DL. Horror autoinflammaticus: the molecular pathophysiology of autoinflammatory disease (*). Annu Rev Immunol. 2009; 27:621–668. [PubMed: 19302049]

2. Aksentijevich I, et al. An autoinflammatory disease with deficiency of the interleukin-1-receptor antagonist. N Engl J Med. 2009; 360:2426–2437. [PubMed: 19494218]

3. McDermott MF, et al. Germline mutations in the extracellular domains of the 55 kDa TNF receptor, TNFR1, define a family of dominantly inherited autoinflammatory syndromes. Cell. 1999; 97:133–144. [PubMed: 10199409]

4. Puel A, Picard C, Ku CL, Smahi A, Casanova JL. Inherited disorders of NF-kappaB-mediated immunity in man. Curr Opin Immunol. 2004; 16:34–41. [PubMed: 14734108]

5. Doffinger R, et al. X-linked anhidrotic ectodermal dysplasia with immunodeficiency is caused by impaired NF-kappaB signaling. Nat Genet. 2001; 27:277–285. [PubMed: 11242109]

6. Courtois G, et al. A hypermorphic IkappaBalpha mutation is associated with autosomal dominant anhidrotic ectodermaldysplasia and T cell immunodeficiency. J Clin Invest. 2003; 112:1108–1115. [PubMed: 14523047]

7. Casanova JL, Abel L, Quintana-Murci L. Human TLRs and IL-1Rs in host defense: natural insights from evolutionary, epidemiological, and clinical genetics. Annu Rev Immunol. 2011; 29:447–491. [PubMed: 21219179]

8. von Bernuth H, et al. Pyogenic bacterial infections in humans with MyD88 deficiency. Science. 2008; 321:691–696. [PubMed: 18669862]

9. Picard C, et al. Pyogenic bacterial infections in humans with IRAK-4 deficiency. Science. 2003; 299:2076–2079. [PubMed: 12637671]

10. Picard C, et al. Clinical features and outcome of patients with IRAK-4 and MyD88 deficiency. Medicine (Baltimore). 2010; 89:403–425. [PubMed: 21057262]

11. Casanova JL, Abel L. Inborn errors of immunity to infection: the rule rather than the exception. J Exp Med. 2005; 202:197–201. [PubMed: 16027233]

12. Casanova JL, Abel L. Primary immunodeficiencies: a field in its infancy. Science. 2007; 317:617–619. [PubMed: 17673650]

13. Picard C, Casanova JL, Puel A. Infectious diseases in patients with IRAK-4, MyD88, NEMO, or I{kappa}B{alpha} deficiency. Clin Microbiol Rev. 2011; 24:490–497. [PubMed: 21734245]

14. von Bernuth H, et al. Septicemia without sepsis: inherited disorders of nuclear factor-kappa B-mediated inflammation. Clin Infect Dis. 2005; 41 (Suppl 7):S436–439. [PubMed: 16237643]

15. Ombrello MJ, et al. Cold urticaria, immunodeficiency, and autoimmunity related to PLCG2 deletions. N Engl J Med. 2012; 366:330–338.10.1056/NEJMoa1102140 [PubMed: 22236196]

16. Tokunaga F, et al. Involvement of linear polyubiquitylation of NEMO in NF-kappaB activation. Nat Cell Biol. 2009; 11:123–132. [PubMed: 19136968]

17. Iwai K, Tokunaga F. Linear polyubiquitination: a new regulator of NF-kappaB activation. EMBO Rep. 2009; 10:706–713. [PubMed: 19543231]

18. Vissers LE, Veltman JA, van Kessel AG, Brunner HG. Identification of disease genes by whole genome CGH arrays. Hum Mol Genet. 2005; 14(Spec No 2):R215–223. [PubMed: 16244320]

19. Byun M, et al. Whole-exome sequencing-based discovery of STIM1 deficiency in a child with fatal classic Kaposi sarcoma. J Exp Med. 2010; 207:2307–2312. [PubMed: 20876309]

20. Bolze A, et al. Whole-exome-sequencing-based discovery of human FADD deficiency. Am J Hum Genet. 2010; 87:873–881. [PubMed: 21109225]

21. Kirisako T, et al. A ubiquitin ligase complex assembles linear polyubiquitin chains. EMBOJ. 2006; 25:4877–4887.

22. Ikeda F, et al. SHARPIN forms a linear ubiquitin ligase complex regulating NF-kappaB activity and apoptosis. Nature. 2011; 471:637–641. [PubMed: 21455181]

23. Gerlach B, et al. Linear ubiquitination prevents inflammation and regulates immune signalling. Nature. 2011; 471:591–596. [PubMed: 21455173]

24. Tokunaga F, et al. SHARPIN is a component of the NF-kappaB-activating linear ubiquitin chain assembly complex. Nature. 2011; 471:633–636. [PubMed: 21455180]

25. Tatematsu K, et al. Transcriptional activity of RBCK1 protein (RBCC protein interacting with PKC 1): requirement of RING-finger and B-Box motifs and regulation by protein kinases. Biochem Biophys Res Commun. 1998; 247:392–396. [PubMed: 9642138]

26. Tian Y, et al. RBCK1 negatively regulates tumor necrosis factor-and interleukin-1-triggered NF-kappaB activation by targeting TAB2/3 for degradation. J Biol Chem. 2007; 282:16776–16782. [PubMed: 17449468]

27. Haas TL, et al. Recruitment of the linear ubiquitin chain assembly complex stabilizes the TNF-R1 signaling complex and is required for TNF-mediated gene induction. Mol Cell. 2009; 36:831–844. [PubMed: 20005846]

28. Zhang M, et al. Negative feedback regulation of cellular antiviral signaling by RBCK1-mediated degradation of IRF3. Cell Res. 2008; 18:1096–1104. [PubMed: 18711448]

29. Hostager BS, Kashiwada M, Colgan JD, Rothman PB. HOIL-1L interacting protein (HOIP) is essential for CD40 signaling. PLoS One. 2011; 6:e23061. [PubMed: 21829693]

30. Zak DE, et al. Systems analysis identifies an essential role for SHANK-associated RH domain-interacting protein (SHARPIN) in macrophage Toll-like receptor 2 (TLR2) responses. Proc Natl Acad Sci USA. 2011

31. Picard C, Puel A, Bustamante J, Ku CL, Casanova JL. Primary immunodeficiencies associated with pneumococcal disease. Curr Opin Allergy Clin Immunol. 2003; 3:451–459. [PubMed: 14612669]

32. Greten FR, et al. NF-kappaB is a negative regulator of IL-1beta secretion as revealed by genetic and pharmacological inhibition of IKKbeta. Cell. 2007; 130:918–931. [PubMed: 17803913]

33. Seymour RE, et al. Spontaneous mutations in the mouse Sharpin gene result in multiorgan inflammation, immune system dysregulation and dermatitis. Genes Immun. 2007; 8:416–421. [PubMed: 17538631]

34. HogenEsch H, Janke S, Boggess D, Sundberg JP. Absence of Peyer's patches and abnormal lymphoid architecture in chronic proliferative dermatitis (cpdm/cpdm) mice. J Immunol. 1999; 162:3890–3896. [PubMed: 10201907]

35. HogenEsch H, et al. Increased expression of type 2 cytokines in chronic proliferative dermatitis (cpdm) mutant mice and resolution of inflammation following treatment with IL-12. Eur J Immunol. 2001; 31:734–742. [PubMed: 11241277]

36. Liang Y, Seymour RE, Sundberg JP. Inhibition of NF-kappaB signaling retards eosinophilic dermatitis in SHARPIN-deficient mice. J Invest Dermatol. 2011; 131:141–149. [PubMed: 20811394]

37. Moses SW, Parvari R. The variable presentations of glycogen storage disease type IV: a review of clinical, enzymatic and molecular studies. Curr Mol Med. 2002; 2:177–188. [PubMed: 11949934]

38. Bruno C, et al. Clinical and genetic heterogeneity of branching enzyme deficiency (glycogenosis type IV). Neurology. 2004; 63:1053–1058. [PubMed: 15452297]

39. Pellissier JF, de Barsy T, Bille J, Serratrice G, Toga M. Polysaccharide (amylopectin-like) storage myopathy histochemical ultrastructural and biochemical studies. Acta Neuropathol Suppl. 1981; 7:292–296. [PubMed: 6939255]

40. Ewert R, et al. Glycogenosis type IV as a rare cause of cardiomyopathy-report of a successful heart transplantation. Z Kardiol. 1999; 88:850–856. [PubMed: 10552189]

41. Vernia S, Rubio T, Heredia M, Rodriguez de Cordoba S, Sanz P. Increased endoplasmic reticulum stress and decreased proteasomal function in lafora disease models lacking the phosphatase laforin. PLoS One. 2009; 4:e5907. [PubMed: 19529779]

42. Lesca G, et al. Novel mutations in *EPM2A* and *NHLRC1* widen the spectrum of Lafora disease. Epilepsia. 2010; 51:1691–1698. [PubMed: 20738377]

43. Monaghan TS, Delanty N. Lafora disease: epidemiology, pathophysiology and management. CNS Drugs. 2010; 24:549–561. [PubMed: 20527995]

44. Li H, Durbin R. Fast and accurate short read alignment with Burrows-Wheeler transform. Bioinformatics. 2009; 25:1754–1760. [PubMed: 19451168]

45. McKenna A, et al. The Genome Analysis Toolkit: a MapReduce framework for analyzing next-generation DNA sequencing data. Genome Res. 2010; 20:1297–1303. [PubMed: 20644199]

46. Li H, et al. The Sequence Alignment/Map format and SAMtools. Bioinformatics. 2009; 25:2078–2079. [PubMed: 19505943]

47. Smahi A, et al. Genomic rearrangement in NEMO impairs NF-kappaB activation and is a cause of incontinentia pigmenti. The International Incontinentia Pigmenti (IP) Consortium. Nature. 2000; 405:466–472. [PubMed: 10839543]

48. Chaussabel D, et al. A modular analysis framework for blood genomics studies: application to systemic lupus erythematosus. Immunity. 2008; 29:150–164. [PubMed: 18631455]
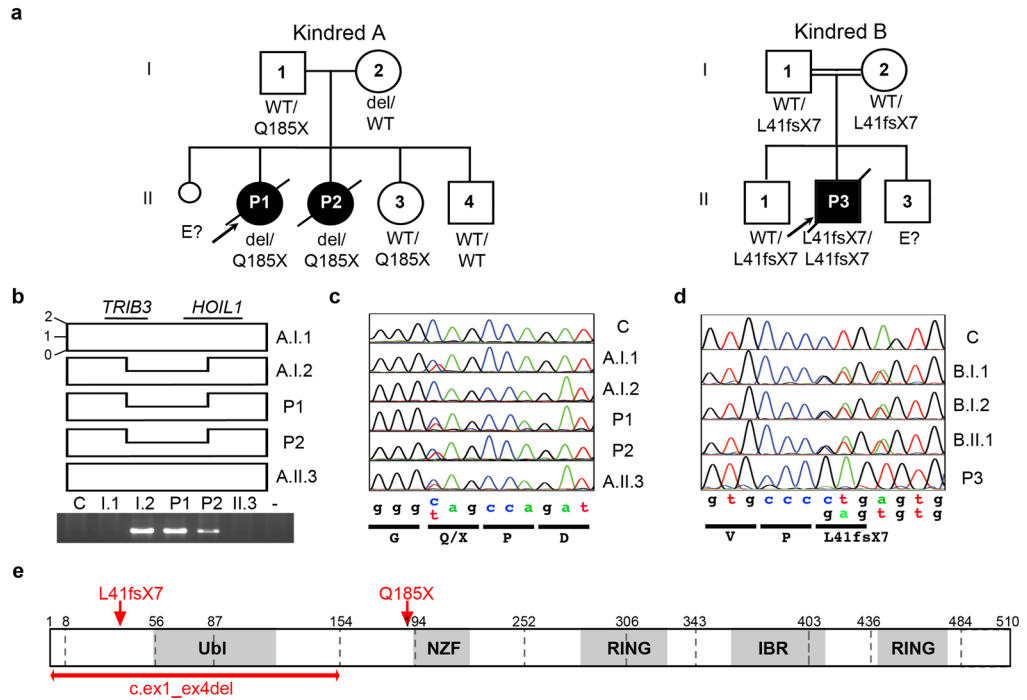
Figure 1. Two kindreds with autosomal recessive *HOIL1* deficiency
a) Pedigree of kindred A, showing the segregation of the 31.799 kb deletion of chromosome 20 (del: *TRIB3*:g.-1272_*HOIL1*:g.9780del) encompassing *TRIB3* and *HOIL1*, and the nonsense c.553 C>T, p.Q185X mutant allele in *HOIL1*. Pedigree of kindred B, showing the segregation of the *HOIL1* deletion c.121_122delCT, p.L41fsX7. The arrow indicates the index case. **b)** Schematic representation of the deletion encompassing the two genes, with the loss of one copy of the allele from individuals A.I.2, P1 and P2. In the lower panel, a PCR-based approach involving amplification of a 1.235 kb fragment with genomic *TRIB3* and *HOIL1* primers reveals the deletion. **c–d)** *HOIL1* DNA sequence electropherograms, for a control and the patients **c)** from kindred A, for the region corresponding to the nonsense mutation and **d)** from kindred B, for the region corresponding to the deletion. **e)** Schematic diagram of the HOIL-1 protein. Ubiquitin-like (Ubl), novel zinc-finger (NZF), ring (RING) and in-between RING (IBR) domains are shaded in gray. Arrows indicate the nonsense and deletion mutations and the double arrow indicates the deletion of the first four exons in *HOIL1*. Exon boundaries are indicated by vertical dashed bars and amino-acid positions are numbered.
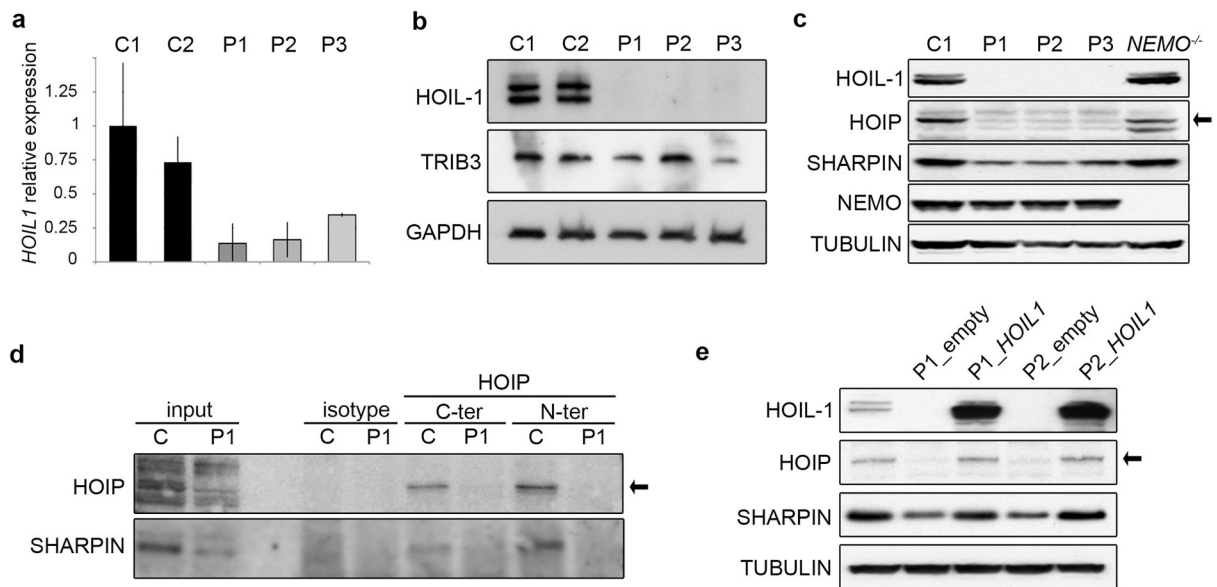
Figure 2. HOIL-1 complete deficiency
a) Relative expression of *HOIL1* in SV40-immortalized fibroblasts from controls (C1 and C2) and patients (P1, P2 and P3). **b)** HOIL-1 and TRIB3 immunoblots of total cell extracts from SV40-immortalized fibroblasts derived from controls and patients. **c)** Low levels of HOIP and SHARPIN in the absence of HOIL-1 in SV40-immortalized fibroblasts. **d)** No HOIP-SHARPIN co-immunoprecipitates can be detected in HOIL-1-deficient fibroblasts. Immunoprecipitation experiments were performed with either control mouse IgGs (isotype) or mouse antibodies against the N-terminus or C-terminus of HOIP in control or P1 patient-derived fibroblasts. HOIP and co-immunoprecipitated SHARPIN were detected by immunoblotting. **e)** Re-expression of HOIL-1 in fibroblasts from patients restores HOIP and SHARPIN protein levels. A retrovirus-based strategy was used for stable re-expression of the wt *HOIL1* allele in fibroblasts from P1 and P2. Fibroblasts infected with empty viruses were used as controls. Data are representative of three experiments (a), four experiments (b), three experiments (c), three experiments (d) or four experiments (e).
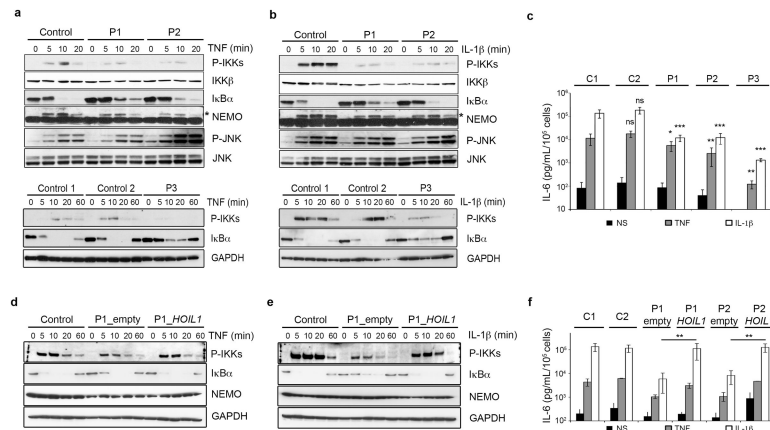
Figure 3. HOIL-1 is required for full TNF-α and IL-1β-induced activation of NF-κB in HOIL-1-deficient fibroblasts

a) Impaired NF-κB activation in response to TNF. Time-course of TNF-stimulated SV40-immortalized fibroblasts, showing impaired IKK kinase phosphorylation, lower levels of NEMO ubiquitination (indicated by an asterisk) and slower IκBα degradation in patients than in controls. JNK phosphorylation in response to TNF is identical in control and patient cells. **b**) Impaired NF-κB activation in response to IL-1β. Time-course of IL-1β-stimulated SV40-immortalized fibroblasts showing impaired IKK kinase phosphorylation (upper panel), lower levels of NEMO ubiquitination (indicated by an asterisk) and slower IκBα degradation in patients than in the controls. JNK phosphorylation in response to IL-1β is identical in control and patient cells. **c**) Low levels of IL-6 production in response to TNF and IL-1β in SV40-immortalized fibroblasts from HOIL-1-deficient patients (P1, P2, P3). All numerical data are means ± SEM. * p<0.05, ** p<0.01, *** p<0.001, ns, not significant. **d–e**) Re-expression of HOIL-1 restores the TNF- and IL-1β-induced activation of NF-κB. The kinetics of TNF and IL-1β stimulation in the indicated cell lines was followed by determining the levels of phospho-IKKs, IκB α and NEMO by immunoblotting. GAPDH was used as a control. **f**) HOIL-1 complementation restores TNF-and IL-1β-induced IL-6 production in fibroblasts from P1 and P2. IL-6 levels in the supernatants of mock-, TNF- and IL-1β-treated cell lines were assayed by ELISA. All numerical data are means ± SEM. (** p<0.01). Data are representative of three experiments (a,b), three experiments (c), two experiments (d,e) or three experiments (f).
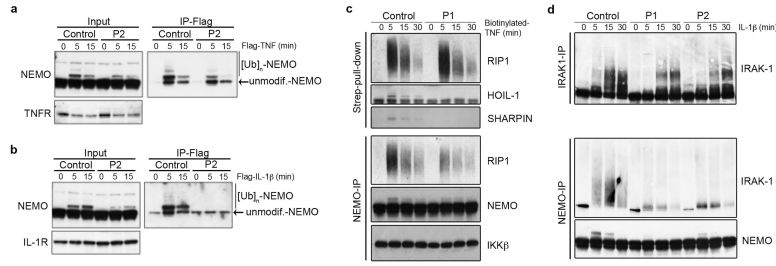
Figure 4. Impaired recruitment of NEMO to cytokine receptors in the patients' fibroblasts
a) HOIL-1 deficiency impairs the recruitment of NEMO to the TNF-RSC. Flag-tagged TNF was used to activate and isolate the TNF-RSC. Cells were lysed, TNF-RSC was purified on Flag-affinity resin and complex-associated NEMO was analyzed by immunoblotting. **b)** HOIL-1 deficiency abolishes NEMO recruitment to the IL-1-RSC. The same strategy as in a) was used, except that Flag-tagged IL-1β was used to stimulate the cells and to isolate the IL-1-RSC. The abundance of TNFR (a) and IL-1R (b), assessed by immunoblotting, was similar in control and patient-derived fibroblasts. **c)** HOIL-1 deficiency impairs the interaction between NEMO and polyubiquitinated RIP1 in response to TNF. NEMO (NEMO-IP) was immunoprecipitated from lysates of control and patient fibroblasts treated with biotinylated TNF and analyzed by immunoblotting for NEMO, RIP1, and IKKβ. The total amount of the ubiquitinated forms of RIP1 associated with the TNF-RSC was evaluated by streptavidin pulldown followed by immunoblotting for RIP1. **d)** HOIL-1 deficiency impairs the interaction between NEMO and polyubiquitinated IRAK-1 in response to IL-1β. NEMO and IRAK-1 were immunoprecipitated from lysates of IL-1β-treated fibroblasts and subjected to western blotting for NEMO or IRAK-1 as indicated. These data are representative of three experiments.
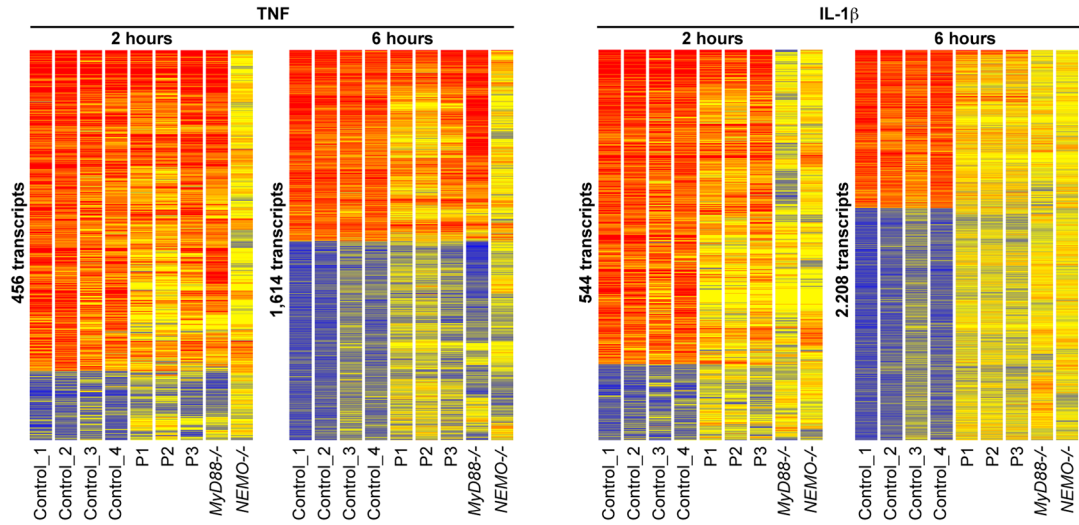
Figure 5. Transcriptome analysis of TNF or IL-1β stimulation of primary fibroblasts
Primary fibroblasts from four healthy donors, P1, P2, P3, MyD88- and NEMO-deficient
cells were stimulated with TNF or IL-1β for 2 and 6 hours. Stimulated samples were
normalized with respect to the corresponding non stimulated reference sample. The heat
maps represent hierarchically clustered transcripts displaying up- or downregulation by a
factor of at least two in stimulated healthy control samples (averaged).
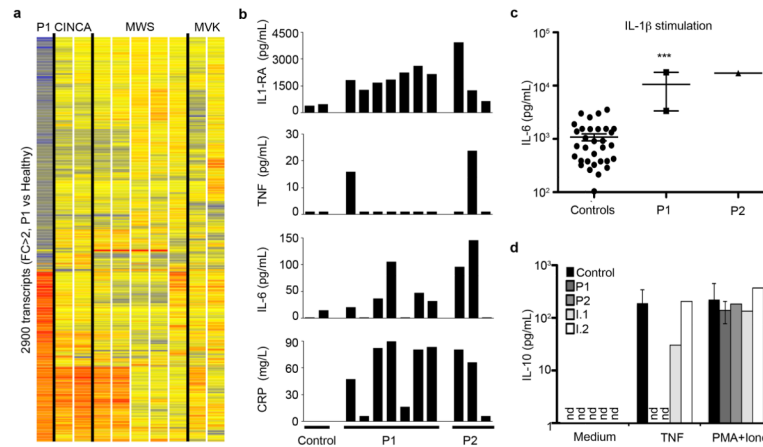
Figure 6. Whole blood analysis reveals a new hyperinflammatory disorder in HOIL-1-deficient patients

a) Transcriptional profiles of whole blood from patients with hyperinflammatory conditions (CINCA, MWS, MVK) and HOIL-1-deficient patients. Comparison of the transcriptional profile of P1 with those of 41 healthy age-matched children (not shown) and other patients with CAPS (2 CINCA, 5 MWS and 2 MVK patients). P1 presented a distinct pattern of gene expression in the blood, with 2,900 transcripts up- or downregulated by a factor of more than two with respect to healthy controls. Red, blue and yellow indicate a relative increase, decrease and no change in expression levels respectively. Samples are ordered by donor: HOIL-1-deficient patient (P1, lane 1), CINCA patients (lanes 2–3), MWS patients (lanes 4–8) and MVK-deficient patients (lanes 9–10). **b)** Quantification of various cytokines in plasma samples. The amounts of IL-1RA (an IL-1 antagonist), TNF, IL-6 and CRP were determined in plasma samples from healthy donors, P1 and P2 taken at various ages. Individuals with CRP concentrations above 3 mg/ml were considered to have an inflammatory condition. **c)** IL-6 secretion by whole-blood cells from 30 healthy donors and HOIL-1-deficient patients (P1, P2), treated with IL-1β for 48 hours. All numerical data are means ± SEM, *** $p < 0.001$ **d)** IL-10 secretion by whole-blood cells from healthy donors and HOIL-1-deficient patients (P1, P2) and the heterozygous parents (I.1, I.2), activated by incubation with TNF or PMA+ionomycin for 48 hours. nd: not detectable
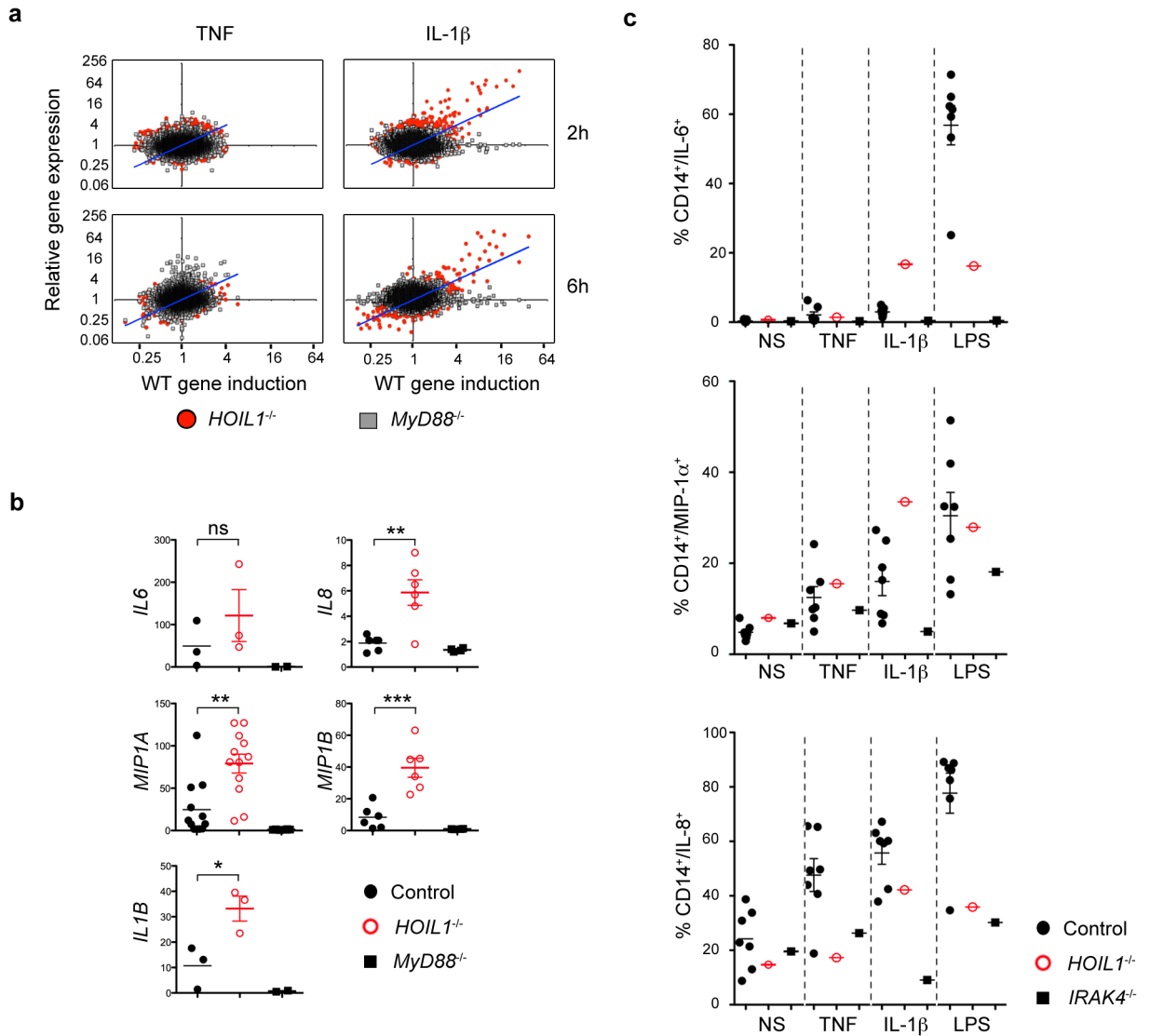
Figure 7. HOIL-1-deficient monocytes display hyperproduction of IL-6 upon IL-1β stimulation
a) Transcriptional profile of leukocytes from P1, P2 and P3 after 2 and 6 hours of stimulation by TNF or IL-1β. The median gene expression in HOIL-1- or MyD88-deficient patients (*y*-axis) was plotted against the median gene expression sorted by ascending order of fold induction in the healthy controls (two of whom were age-matched). Each dot corresponds to one probe. **b**) Levels of *IL6*, *IL8*, *MIP1A*, *MIP1B* and *IL1B* mRNA in 3 healthy controls, 3 HOIL-1- (P1, P2 and P3) and 2 MyD88-deficient patients, extracted from the microarray data. Each dot corresponds to one probe in one individual. The number of probes per gene is 1 for *IL6* and *IL1B*, 2 for *MIP1B* and *IL8* and 4 for *MIP1A*. The non parametric Mann-Whitney test was used for statistical analysis (* *p*<0.1, ** *p*<0.05, *** *p*<0.005). **c**) Cytokine production in CD14⁺ cell subsets determined by intracellular staining of stimulated PBMCs. PBMCs from P2, 7 healthy controls and 1 IRAK-4-deficient patient were stimulated with TNF, IL-1β or LPS. The secretory pathways were concomitantly blocked with monensin and brefeldin A. Twelve hours after stimulation, the cells were immunolabeled with antibodies against CD14 and then permeabilized to assess the production of IL-6, MIP-1α and IL-8. Cells were analyzed by flow cytometry. (*n*=1).